EBioMedicine 7 (2016) 50–61

Contents lists available at ScienceDirect

EBioMedicine

journal homepage: www.ebiomedicine.com

Research Paper

Co-targeting hexokinase 2-mediated Warburg effect and ULK1-dependent autophagy suppresses tumor growth of *PTEN*- and *TP53*-deficiency-driven castration-resistant prostate cancer

Lei Wang [a,1], Ji Wang [a,1], Hua Xiong [a], Fengxia Wu [a], Tian Lan [a], Yingjie Zhang [a], Xiaolan Guo [a], Huanan Wang [a], Mohammad Saleem [a], Cheng Jiang [b], Junxuan Lu [b], Yibin Deng [a,*]

[a] *Laboratory of Cancer Genetics, The University of Minnesota Hormel Institute, Austin, MN, 55912, USA*
[b] *Department of Pharmacology, Penn State College of Medicine, Hershey, PA, 17033, USA*

ARTICLE INFO

Article history:
Received 31 July 2015
Received in revised form 9 March 2016
Accepted 16 March 2016
Available online 19 March 2016

Keywords:
Warburg effect
Autophagy
PTEN
TP53
Hexokinase 2
AMPK
ULK-1
MCL-1
2-Deoxy-glucose
Chloroquine
Androgen receptor
Castration-resistant prostate cancer
Genetically-engineered mouse model

ABSTRACT

Currently, no therapeutic options exist for castration-resistant prostate cancer (CRPC) patients who have developed resistance to the second generation anti-androgen receptor (AR) axis therapy. Here we report that co-deletion of *Pten* and *p53* in murine prostate epithelium, often observed in human CRPC, leads to AR-independent CRPC and thus confers *de novo* resistance to second generation androgen deprivation therapy (ADT) in multiple independent yet complementary preclinical mouse models. In contrast, mechanism-driven co-targeting hexokinase 2 (HK2)-mediated Warburg effect with 2-deoxyglucose (2-DG) and ULK1-dependent autophagy with chloroquine (CQ) selectively kills cancer cells through intrinsic apoptosis to cause tumor regression in xenograft, leads to a near-complete tumor suppression and remarkably extends survival in *Pten*−/*p53*-deficiency-driven CRPC mouse model. Mechanistically, 2-DG causes AMPK phosphorylation, which in turn inhibits mTORC1-S6K1 translation signaling to preferentially block anti-apoptotic protein MCL-1 synthesis to prime mitochondria-dependent apoptosis while simultaneously activates ULK1-driven autophagy for cell survival to counteract the apoptotic action of anti-Warburg effect. Accordingly, inhibition of autophagy with CQ sensitizes cancer cells to apoptosis upon 2-DG challenge. Given that 2-DG is recommended for phase II clinical trials for prostate cancer and CQ has been clinically used as an anti-malaria drug for many decades, the preclinical results from our proof-of-principle studies *in vivo* are imminently translatable to clinical trials to evaluate the therapeutic efficacy by the combination modality for a subset of currently incurable CRPC harboring *PTEN* and *TP53* mutations.

1. Introduction

Prostate cancer strikes one in six men and is the second leading cause of cancer-related deaths in men after lung cancer in the United States. Prostate cancer arises mainly from prostatic intraepithelial neoplasia (PIN), a precursor lesion that ultimately progresses to adenocarcinoma and systemic metastasis (DeMarzo et al., 2003). Conventional androgen deprivation therapy (ADT) by surgical and/or chemical castration remains the standard of care for metastatic prostate cancer. Unfortunately, these prostate cancers invariably develop resistance to ADT and progress to a more aggressive castration-resistant prostate cancer (CRPC) within 18–24 months. Chemotherapy with docetaxel (Petrylak et al., 2004) or its derivative carbazitaxel after development of docetaxel resistance (de Bono et al., 2010) offers a 3–4 months survival benefit for CRPC patients. The discovery that persistent androgen receptor (AR) signaling plays a crucial role in the progression of CRPC leads to "second generation" ADT modalities (Chen et al., 2004; Tran et al., 2009), such as the Food and Drug Administration-approved androgen synthesis blocker abiraterone (2011, FDA) and the second generation of AR signaling inhibitor enzalutamide (formerly MDV3100) (2012, FDA), which have demonstrated efficacy against chemotherapy-resistant CRPC with median increase in survival of 4–5 months (de Bono et al., 2011; Ryan et al., 2013; Scher et al., 2010, 2012). However, nearly all CRPC patients inevitably develop acquired resistance to the second generation anti-AR signaling axis treatments within ~6–12 months (Claessens et al., 2014). Significantly, approximately 20 to 40% of CRPC patients do not initially respond to abiraterone or enzalutamide with respect to prostate-specific antigen (PSA) levels (de Bono et al., 2011; Ryan et al., 2013; Scher et al., 2010, 2012), suggesting a subset of CRPC possesses *de novo*/innate resistance to next-generation anti-AR axis therapies. Therefore, understanding the molecular mechanisms underlying the innate/acquired resistance to

* Corresponding author at: The University of Minnesota Hormel Institute, 801 16th Ave NE, Austin, MN 55912, USA.
E-mail address: yideng@hi.umn.edu (Y. Deng).
[1] These authors contributed equally to this work.

http://dx.doi.org/10.1016/j.ebiom.2016.03.022

current anti-AR axis therapies has important clinical implications towards a better stratification of CRPC patients, rational designing of innovative and cost-effective personalized therapeutic strategies for them, as well as the discovery of novel therapeutics for overcoming resistance.

Beside the AR signaling axis, accumulating evidence suggests that important fundamental genetic alterations, such as loss of tumor suppressor genes *PTEN* and/or *TP53*, might play a crucial role in the development of CRPC (Chen et al., 2005; Lunardi et al., 2013; Wang et al., 2014). Recent advances in whole-genome/exome sequencing analyses reveal that *PTEN* and *TP53* are often co-deleted or co-mutated in lethal CRPC (Grasso et al., 2012). A systematic and multi-institutional study of metastatic CRPC specimens has shown that 60 cases (40%) have *PTEN* mutations, 75 cases (50%) have *TP53* mutations, and 34 cases (22.7%) have co-occurrence of *PTEN* and *TP53* mutations in the 150 cases of metastatic CRPC (Robinson et al., 2015). Importantly, tracking the clonal origin of lethal prostate cancer through patient samples collected during tumor progression and at the time of death identified that the lethal metastatic clone arose from primary prostate cancer cells carrying *PTEN* deletion and mutant *p53* (Haffner et al., 2013). Systems bioinformatics analyses estimate that prostate cancers with combined loss of *PTEN* and *TP53* make up 11% of highly aggressive prostate cancers and they bestow the worst survival outcome for patients (Markert et al., 2011). Strikingly, 4 out of 6 CRPC patients-derived prostate cancer organoid lines carry co-mutations of *PTEN/TP53* (Gao et al., 2014). In support of the clinical findings that co-deletion/— mutation of *PTEN/TP53* in prostate epithelial cells plays a causal role in prostate tumorigenesis, mouse genetic studies suggest that *Pten* deletion in prostate epithelial cells primarily initiates PIN, whereas *p53* loss in prostate epithelial cells is not sufficient to cause any distinguishable morphological phenotypes *in vivo*. However, double deletion of *Pten* and *p53* in murine prostate epithelial cells leads to invasive prostate cancer (Chen et al., 2005; Wang et al., 2014) which develops into CRPC with innate or *de novo* resistance to conventional ADT *in vivo* (Lunardi et al., 2013). Thus, utilizing the *Pten* —/— *p53*-deficient CRPC model that recapitulates the salient features of a subset of human CRPC to explore effective and selective means of killing prostate cancer cells *in vivo* is a critical step to develop novel therapeutic strategies to successfully treat the CRPC patients harboring *PTEN/TP53* mutations.

On the basis of our genetic findings that hexokinase 2 (HK2)-mediated aerobic glycolysis, known as the Warburg effect, drives prostate tumor growth in xenograft model bearing *Pten* —/*p53*-deficient murine or human prostate cancer cells (Wang et al., 2014), we designed preclinical studies to determine the therapeutic efficacy on *Pten* —/*p53*-deficiency-driven prostate tumorigenesis by pharmacologically co-targeting HK2-mediated Warburg effect and ULK1-dependent autophagy in genetic mouse models. We report here that pharmacologic inhibition of HK2 enzymatic activity with 2-deoxyglucose (2-DG) phosphorylates AMPK which inhibits mTORC1-S6K1 translation axis to preferentially reduce anti-apoptotic protein MCL-1 synthesis to prime intrinsic apoptosis while simultaneously induces ULK1-dependent pro-survival autophagy to counteract the apoptotic action of anti-Warburg effect. Accordingly, co-targeting HK2-mediated aerobic glycolysis with 2-DG and ULK1-driven autophagy with chloroquine (CQ) selectively kills cancer cells through apoptosis to cause significant tumor regression in xenograft, leads to near-complete tumor suppression and significantly extends survival in *Pten* —/*p53*-deficiency-driven CRPC mouse models. Thus, our preclinical studies suggest an innovative and efficacious therapeutic strategy for the subsets of currently incurable CRPC carrying *PTEN* and *TP53* mutations.

2. Results

2.1. Inhibition of HK2-mediated Warburg effect activates AMPK-dependent autophagy

Our previous genetic studies have shown that depletion of HK2 inhibits *Pten* —/*p53*-deficiency-driven prostate cancer growth in xenograft mouse models (Wang et al., 2014). The underlying mechanism is due to reduction of cell proliferation rather than induction of apoptosis. Given that autophagy plays a controversial but important role in response to cancer treatment (Mathew et al., 2007), we examined whether genetic targeting HK2 would regulate autophagy in prostate cancer cells. During autophagy, LC3-I (cytosolic form) is modified by lipids to the faster migrating LC3-II membrane-bound lipidated form, which is conjugated to phosphatidylethanolamine and incorporated into the autophagosomal membrane. Therefore, active autophagy can be measured by monitoring LC3-II by immunohistochemistry (IHC) and Western blots, and by microscopy using fluorescent protein–tagged LC3 (GFP-LC3) (Mizushima et al., 2010). We found that LC3-II detected by IHC was increased in xenografts carrying human *PTEN* —/*p53*-deficient PC3 cells with HK2 depletion by shRNAs (Fig. 1A), suggesting HK2 depletion in PC3 cell-derived xenografts activated autophagy. Since the serine/threonine kinase AMPK plays a crucial role in metabolic stress-induced autophagy (Hardie et al., 2012), we examined whether genetic inhibition of Warburg effect through HK2 depletion is sufficient to induce AMPK-dependent autophagy. HK2 reduction by shRNAs in tumors activated AMPK, as indicated by the phosphorylated AMPKα (the catalytic subunit of AMPK) at threonine 172 (Fig. 1A). Knockdown of AMPKα by shRNA in PC3 cells significantly reduced LC3-II levels as determined by Western blot in HK2-depleted prostate cancer cells (Fig. 1B). Notably, depletion of HK2 in PC3 cells stably expressing GFP-LC3 increased puncta formation of GFP-LC3 (Fig. 1C and D). Conversely, depletion of AMPKα by shRNA dramatically reduced the puncta formation of GFP-LC3 (Fig. 1C and D). These results together suggest that genetic inhibition of HK2-mediated aerobic glycolysis leads to AMPK-dependent autophagy in prostate cancer cells.

We next tested if these genetic phenotypes could be replicated with the pharmacologic inhibition of HK2 enzymatic activity by 2-deoxyglucose (2-DG). As expected, 2-DG inhibited aerobic glycolysis as indicated by the significant reduction of glucose consumption and lactate production in PC3 cells (Fig. 1E and F). 2-DG profoundly reduced cell proliferation (Fig. 1G). Flow cytometry analyses indicated a significant reduction of cells with S phase cells and an increase of cells with G_1 arrest, but no appreciable effect on apoptosis as minimal increase in sub-G_1 population was observed (Fig. 1H). Importantly, 2-DG induced time-dependent increase of LC3-II levels (Fig. S1A, upper panel) and increased the formation of autophagosomes manifested as the increase of GFP-LC3 puncta in PC3 cells stably expressing GFP-LC3 (Fig. S1B and C). As LC3-II accumulation could also occur due to dysfunctional late-autophagic processes such as inhibition of lysosomal degradation, we treated PC3 cells with 2-DG alone or in combination with two lysosomal inhibitors (E64d and pepstatin A) (Mizushima et al., 2010). 2-DG combined with E64d/pepstatin A increased the level of LC3-II compared with cells treated with 2-DG only (Fig. S1A, lower panel). Thus, consistent with our observations from genetic ablation of HK2, pharmacologic inhibition of HK2-mediated aerobic glycolysis with 2-DG in PC3 cells led to a reduction in cell proliferation and an activation of autophagy, but had minimal effects on cell apoptosis.

We then determined whether 2-DG-induced autophagy also depended on AMPK in PC3 cells. 2-DG induced a time-dependent AMPK phosphorylation (Fig. 1I). AMPK knockdown reduced LC3-II in PC3 cells (Fig. 1J) and GFP-LC3 puncta formation in PC3-GFP-LC3 cells upon 2-DG challenge (Fig. 1K). Collectively, these findings support that genetic or pharmacologic targeting HK2-mediated Warburg effect inhibits cancer cell proliferation and promotes AMPK-dependent autophagy with negligible impact on apoptosis.

2.2. Inhibition of autophagy converts 2-DG-induced cell cycle arrest into apoptosis in prostate cancer cells

To dissect the role of AMPK-dependent autophagy in 2-DG-mediated cellular resposes in PC3 cells, we measured cell viability upon genetic or pharmacologic inhibition of autophagy. When the

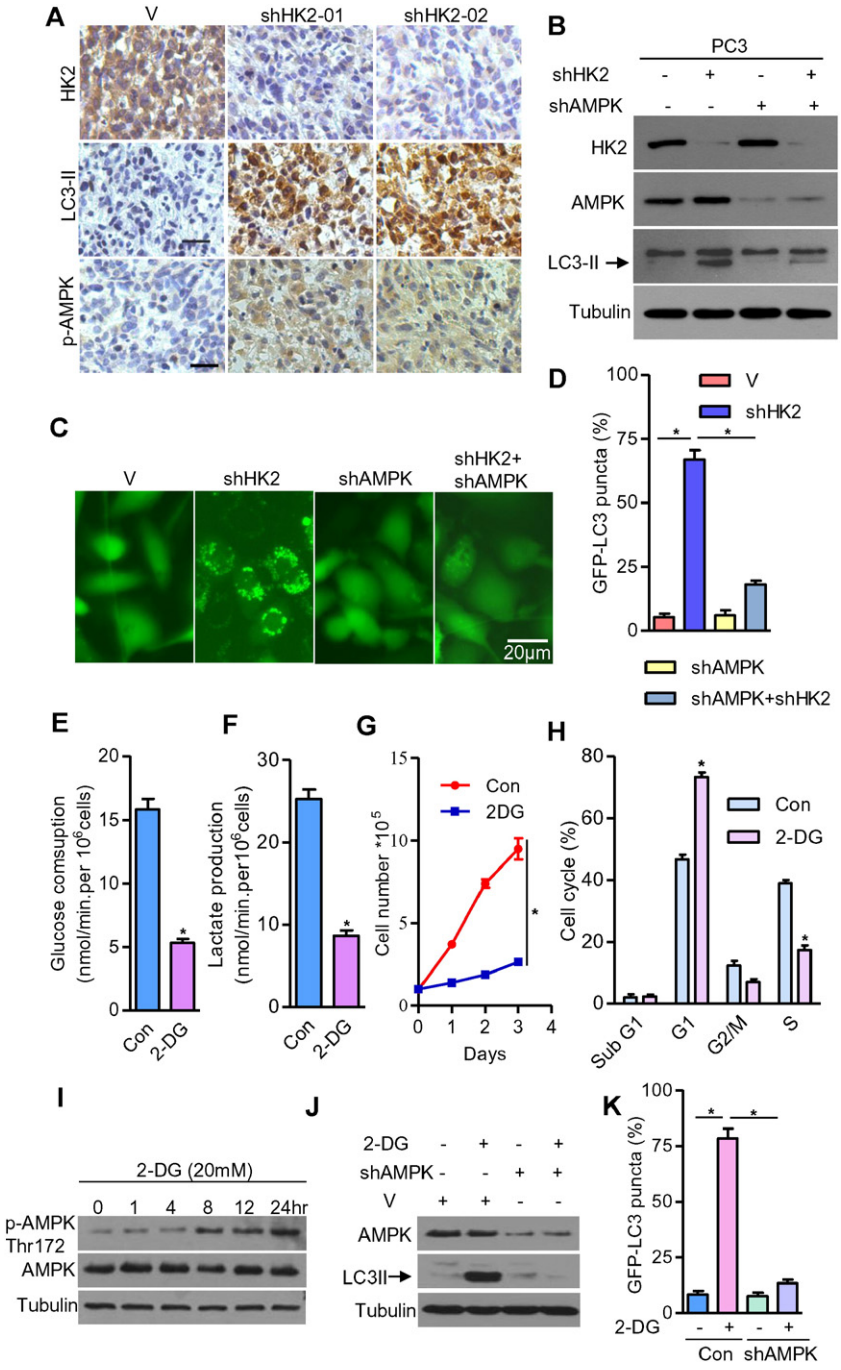

Fig. 1. Targeting HK2 in prostate cancer cells induces AMPK-dependent autophagy. (A–D) Depletion of HK2 activates AMPK-mediated autophagy. (A) Representative images of IHC staining of HK2, LC3-II, and phosphorylated AMPK are shown in xenografts carrying PC3 cells stably expressing scramble or shRNAs for HK2. (B) PC3 cells were transfected with HK2 shRNA (shHK2) and/or AMPK shRNA (shAMPK). Lysates from the cells were immunoblotted by the indicated antibodies. (C) Representative images of GFP-LC3 translocation in PC3-GFP-LC3 cells expressing shRNAs for HK2 and/or AMPK. (D) Quantification of GFP-LC3 translocation from the representative images shown in C. (E–K) Pharmacologic inhibition of HK2 suppresses Warburg effect-mediated cell proliferation and induces AMPK-dependent autophagy. (E) Glucose consumption and (F) lactate production for PC3 cells treated with vehicle only (Con) or 2-DG (20 mM). (G) Cell proliferation and (H) cell cycle distribution determined by flow cytometry in PC3 cells treated with vehicle only or 2-DG. (I) Immunoblots of lysates from PC3 cells treated with 2-DG (20 mM) for the indicated times. (J) Lysates from PC3 cells stably expressing scramble or AMPK shRNA treated with vehicle or 2-DG for 24 h were immunoblotted by the indicated antibodies. (K) Quantification of GFP-LC3 translocation is shown in PC3-GFP-LC3 cells expressing scramble shRNA (Con) and/or AMPK shRNA (shAMPK) upon 2-DG challenge. At least 500 cells were counted for each experimental repeat. For western blot, tubulin was used as a loading control. All data are shown as means ± SEM. *P ≤ 0.01. Scale bar = 50 μm unless otherwise indicated. See also Fig. S1.

autophagy essential genes (Ohsumi, 2001), such as *ATG5*, *ATG7* and *BECLIN1*, were effectively depleted by shRNAs, 2-DG treatment significantly induced prostate cancer cell apoptosis, as demonstrated by the increase of cleaved PARP levels, and a 45% or greater reduction of cell viability (Fig. 2A–C and S2A-C). Knocking down ULK1, a critical downstream target involved in AMPK-regulated autophagy (Kim et al., 2011), cooperated with 2-DG to reduce cell viability and identical results were obtained as PC3 cells expressing shRNAs for *ATG5*, *ATG7* and *BECLIN1* (Fig. 2D and S2D). These data suggest that *PTEN* −/*p53*-deficient PC3 cells utilize AMPK-ULK1-dependent autophagy as a cell survival mechanism against 2-DG-mediated anti-glycolysis treatment. To demonstrate this possibility pharmacologically, we used chloroquine (CQ) to prevent lysosomal fusion with autophagosomes to block autophagy (Rubinsztein et al., 2007). No appreciable cell death was

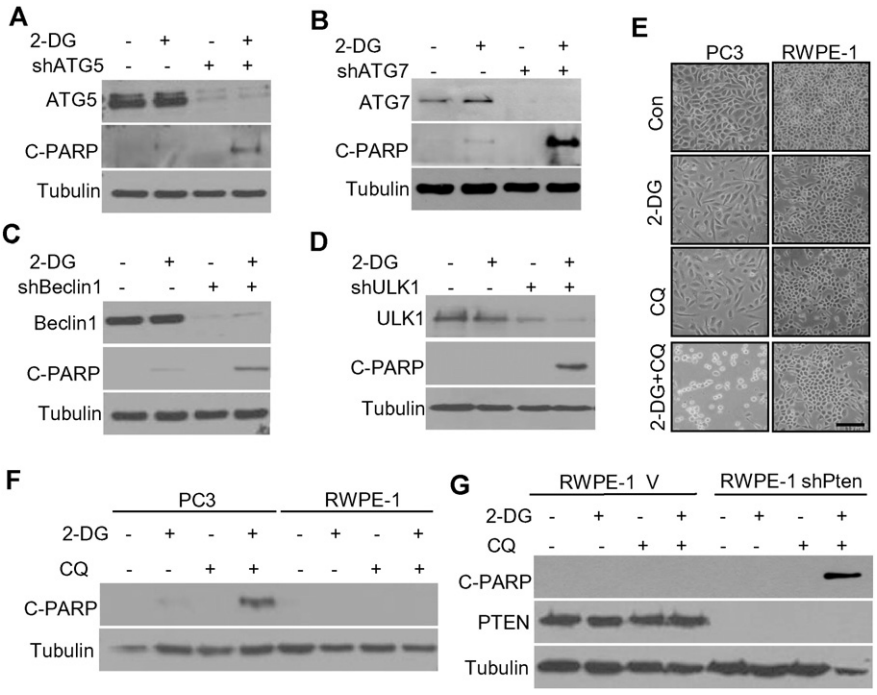

Fig. 2. Inhibition of autophagy converts 2-DG-mediated cell cycle arrest into mitochondria-dependent apoptosis in prostate cancer cells. (A–D) Genetic inhibition of autophagy sensitizes cancer cells to apoptosis with 2-DG. Lysates from PC3 cells expressing shRNAs for ATG5 (A), ATG7 (B), Beclin 1(C), and ULK1 (D) were immunoblotted with the indicated antibodies. (E–I) Pharmacologic inhibition of autophagy by CQ collaborates with 2-DG to induce intrinsic apoptosis. (E) Representative images of phase photomicrographs of PC3 or RWPE-1 cell viability in the absence (Con) or presence of 2-DG (20 mM), CQ (50 μM) or 2-DG plus CQ for 36 h are shown. (F) Lysates from PC3 and RWPE-1 cells upon 2-DG and/or CQ treatment were subject to immunoblotting with the indicated antibodies. (G) Immunoblots of lysates from RWPE-1 cells stably expressing scramble or *PTEN* shRNA upon 2-DG and/or CQ treatment for 48 h. Tubulin serves as a loading control for Western blot. Scale bar = 100 μm. See also Fig. S2.

observed in PC3 cells and the non-transformed human prostate epithelial RWPE-1 cells treated with 2-DG or CQ alone, however, the combination induced remarkable apoptosis in PC3 cells, but not in RWPE-1 cells (Fig. 2E, F and S2E). These findings indicated that the combination therapy preferentially killed prostate cancer cells over non-cancerous prostate epithelial cells. This selectivity might be due to the addiction of *PTEN* −/*p53*-deficient prostate cancer cells to HK2-mediated Warburg effect, and consequently autophagy for cell survival when Warburg effect was inhibited. If true, *PTEN* depletion in the *p53*-inactive, non-tumorigenic RWPE-1 cells should render these genetically-manipulated cells with enhanced HK2 expression (Wang et al., 2014) sensitive to the combination treatment. Indeed, treating *PTEN*-depleted RWPE-1 cells with 2-DG and CQ induced significant apoptosis (Fig. 2G and S2F).

2.3. 2-DG primes mitochondria for apoptosis through AMPK-mTORC1-MCL1 signaling in prostate cancer cells

Given that induction of autophagy compromises apoptosis upon 2-DG-mediated anti-glycolysis treatment, we expect that inhibition of AMPK-dependent autophagy by depletion of AMPK sensitizes cancer cells to 2-DG. Surprisingly, in contrast to ULK1-depleted PC3 cells with 2-DG treatment (Fig. 2D), no appreciable apoptotic PARP cleavage was observed in AMPK-depleted PC3 cells upon 2-DG challenge (Fig. 3A and B). These results prompted us to test the possibility that activation of AMPK with 2-DG initiates a signaling pathway to sensitize cancer cells for apoptosis while induction of AMPK-ULK1-dependent autophagy protects cancer cells from apoptosis. Consistent with earlier studies that activated AMPK inhibits mTORC1 signaling (Hardie et al., 2012), phosphorylation of p70S6K, a critical downstream effector of mTORC1 axis in the regulation of translation (Thoreen et al., 2012), was significantly reduced, mirror opposite of activated AMPK in 2-DG-treated PC3 cells (Fig. 3C). Notably, selective reduction of mitochondrial BCL2 family members of anti-apoptotic protein MCL-1, but not BCL-2 and BCL-xl or pro-apoptotic protein BAX or BAK, was observed in PC3 cells treated with 2-DG (Fig. 3C). Depletion of AMPK significantly attenuated 2-DG-caused reduction of phosphorylated p70S6K and partially restored MCL-1 protein expression (Fig. 3D). However, knockdown of p70S6K reduced MCL-1 protein expression but not mRNA abundance (Fig. 3E and data not shown), consistent with previous observation that MCL-1 can be translationally regulated by mTOR signaling in certain cancer cells (Mills et al., 2008). Moreover, exogenous overexpression of MCL-1 dramatically inhibited apoptosis induced by combination of 2-DG and CQ in PC3 cells (Fig. 3F). These findings collectively indicate that AMPK suppression of mTORC1-p70S6K-MCL-1 axis plays a critical role in transducing 2-DG-induced metabolic stress signal to prime mitochondria for cell death while AMPK induction of ULK1 signaling counteracts the apoptotic action of anti-glycolysis (Fig. 3G). Thus, inhibition of AMPK downstream ULK1-mediated autophagy, but not AMPK itself, favors cell apoptosis caused by reduction of MCL-1 resulting from AMPK suppression of mTORC1 signaling upon 2-DG treatment.

2.4. Pharmacologic co-targeting Warburg effect and autophagy causes tumor regression in xenograft model carrying PC3 cells

On the basis of our aforementioned cell culture findings, we reasoned that co-targeting HK2-mediated Warburg effect with 2-DG and ULK1-dependent autophagy with CQ *in vivo* would induce cancer cell apoptosis to suppress human prostate tumor growth. To this end, we established xenograft model using human PC3 cells. The NSG mice harboring the PC3 tumor xenografts of approximately 50 mm^3 were randomly assigned to the following four groups: PBS (control), 2-DG, CQ, or 2-DG plus CQ. Monotherapy with 2-DG or CQ caused a moderate inhibition of tumor growth, but was incapable of causing tumor regression (Fig. 4A–C). In contrast, combination therapy with 2-DG and CQ caused significant regression of established PC3 tumor xenografts (Fig. 4A–C). Analyses of the PC3 xenografts showed that the percentage of

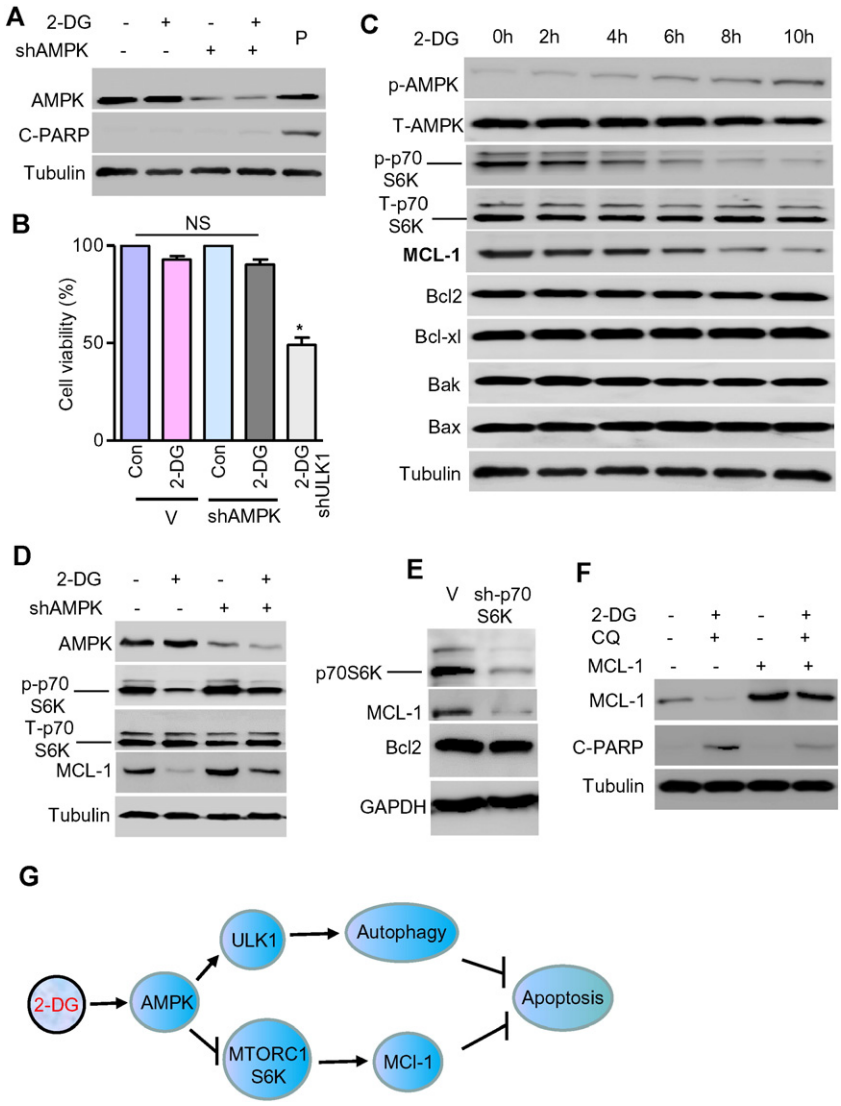

Fig. 3. Activation of AMPK-S6K-MCL-1 Signaling Sensitizes Cancer Cells to Apoptosis upon 2-DG Treatment. (A) Lysates from PC3 cells expressing shRNAs for scramble or AMPK were immunoblotted with the indicated antibodies upon 2-DG treatment. P indicates positive control lysates for cleaved PARP. (B) Quantification of cell viability from PC3 cells stably expressing scramble or *AMPK* shRNA upon 2-DG treatment for 48 h. PC3 cells-shULK1 serves as positive control. (C) Immunoblots of lysates with indicated antibodies from PC3 cells treated with 2-DG at different time courses. (D) Lysates from PC3 cells expressing scramble or *AMPK* shRNAs treated with 2-DG and CQ were immunoblotted by the indicated antibodies. (E) Lysates from PC3 cells expressing scramble or p70S6K1 shRNAs were immunoblotted by the indicated antibodies. (F) Lysates from PC3 cell expressing vector or exogenous MCL-1 treated with vehicle or 2-DG were immunoblotted by the indicated antibodies. (G) Schematic model of 2-DG-induced AMPK phosphorylation regulates autophagy and apoptosis. Tubulin served as a loading control for Western. Data are shown means ± SEM. All the cell viability experiments are repeated three times. *P ≤ 0.01.

cells positive for cleaved caspase 3 was 28% in NSG mice treated with both drugs, while the percentage was only 2.4% and 2.1% in those treated with 2-DG or CQ, respectively (Fig. 4D and F), although inhibition of cell proliferation upon individual treatment was comparable with the combination treatment as evident by significantly decreased Ki-67 positive cells (Fig. 4D and E). Therefore, the combination of 2-DG and CQ *in vivo* causes an effective tumor regression through the induction of cancer cell apoptosis in the xenograft model carrying PC3 cells.

2.5. Loss of Pten and p53 in murine prostate epithelium leads to tumor growth independent of AR signaling in xenograft model

To test whether *Pten* −/*p53*-deficiency confers to murine prostate cancer cells the abilities to develop innate resistance to ADT in xenograft mouse models, the UMN-4240P mouse cell lines derived from *Pten* −/*p53*-deficient prostate tumors (Wang et al., 2014) were injected into the flank of non-castrated and surgically-castrated male NSG mice, and tumor growth was monitored weekly. No difference was observed for tumor size, tumor weight, cellular proliferation marker Ki-67, and apoptotic marker cleaved caspase 3 in xenografts derived from non-castrated and castrated male NSG mice (Fig. S3A–E).

Given that AR plays an important function in the development of CRPC (Chen et al., 2004), we utilized UMN-4240P mouse cancer cells expressing endogenous Ar to determine its role in *Pten*/*p53*-deficiency-driven CRPC *in vivo*. Lentivirus-mediated shRNAs for *Ar* efficiently reduced Ar expression in UMN-4240P cells, but did not affect cell proliferation and/or apoptosis (Figs. S3F and 3G). Importantly, the UMN-4240P cells stably expressing lentivirus-mediated shRNAs for *Ar* or empty vector (control) implanted into the flanks of castrated male NSG mice grew at identical rate as the vector-infected controls as indicated by tumor size and weight (Figs. S3H and 3I). No difference was observed for Ki-67 and cleaved caspase 3 in xenograft tumors harboring vector or shRNAs for *Ar* (Fig. S3J–L). Consistent with the genetic studies, pharmacologic inhibition of the AR signaling axis by the second generation AR antagonist drug enzalutamide had no detectable effect on the inhibition of cell proliferation and tumor growth in xenograft mouse models, as evaluated by tumor growth (Fig. 5A–C). These findings together support that *Pten* −/*p53*-deficiency confers to the prostate cancer cells intrinsic

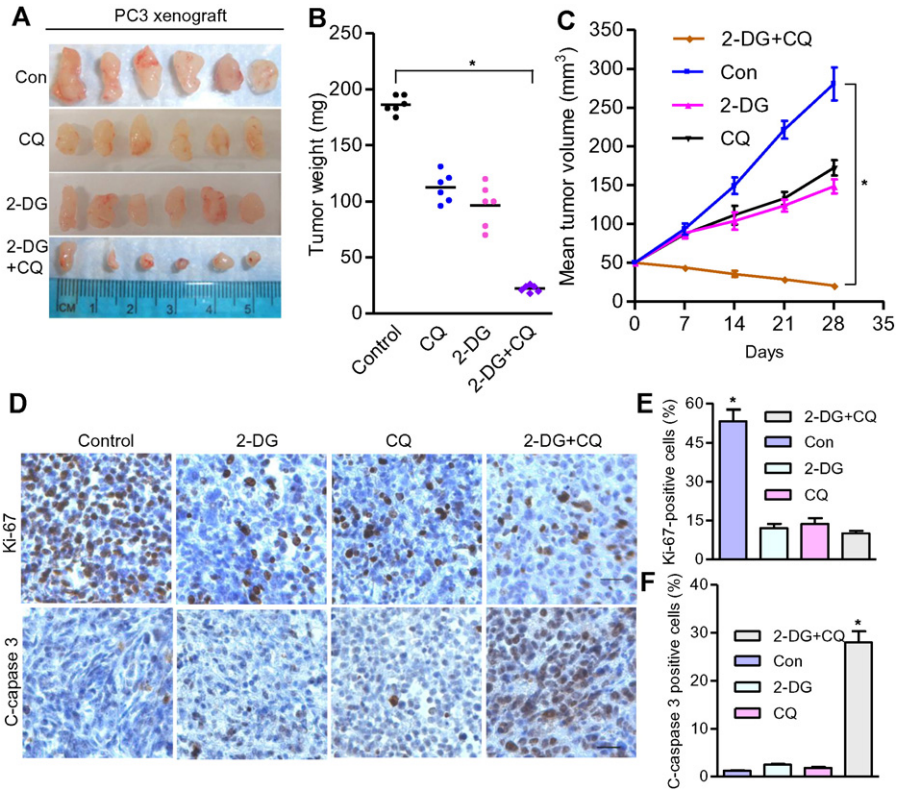

Fig. 4. Co-targeting Warburg effect and autophagy causes tumor regression in human CRPC xenograft mouse model. (A) Representative images of tumor sizes after 4 weeks of treatment as indicated. (B) Quantification of tumor weight of PC3 xenografts as shown in (A). The horizontal line represents the average tumor weights for each group. (C) Tumor volumes were measured once per week and plotted as a function of time. Each data point represents average tumor volume for the indicated treatment group. (D) Representative IHC images of Ki-67 and cleaved caspase 3 (C-caspase 3) in PC3 xenografts from (A) are shown to assess tumor cell proliferation and apoptosis. (E) Quantification of Ki-67 positive cells in PC3 xenografts shown in (D). (F) Quantification of cleaved caspase 3 positive cells in PC3 xenografts shown in (D). All data are means ± SEM. *P ≤ 0.01. Scale bar = 50 μm.

resistance to ADT and leads to prostate tumor growth bypassing the requirement of AR signaling axis in xenograft.

2.6. Co-targeting Warburg effect and autophagy inhibits tumor growth in xenograft model carrying murine Pten −/p53-deficient prostate cancer cells

Since our genetic studies have shown that HK2 is required for *Pten*/*p53*-deficiency-driven tumor growth of UMN-4240P cells (Wang et al., 2014), we speculated that pharmacologic inhibition of HK2-mediated Warburg effect with 2-DG and ULK1-dependent autophagy with CQ should suppress CRPC tumor growth in xenograft models carrying UMN-4240P cells. To this end, male NSG mice bearing UNN-4240P tumor xenografts of approximately 100 mm^3 were randomly assigned to the following two groups: PBS (control) and 2-DG plus CQ. Combination therapy with 2-DG and CQ reduced tumor size and weight in treated mice compared with control group (Fig. 5D and E). Analyses of the residual xenograft tumors showed that the percentage of cancer cells positive for Ki-67 and cleaved caspase 3 was about 20% and 12% in NSG mice treated with both drugs, while the percentage is around 65% and less than 2% in those control mice group treated with PBS, respectively (Fig. 5F–H).

2.7. Co-targeting Warburg effect and autophagy robustly suppresses Pten −/p53-deficiency-driven CRPC in genetic mouse model

To validate the *de novo* CRPC phenotype reported by Lunardi A et al. as the result of double loss of *Pten* and *p53* in murine prostate epithelium, which was completely resistant to surgical castration and the classical AR antagonist drug bicalutamide (Lunardi et al., 2013), we castrated *Pten*- and *p53*-double deficient mice by surgically removing the testes and epididymis at 12 weeks of age. Castration did not inhibit tumor growth and progression, as demonstrated by no histopathology changes and no significant reduction of prostate tumor weight in the castrated *Pten −/p53*-deficient mice compared to the non-castrated controls (Figs. S4A and 4B). Given the advantage of second generation anti-AR drug enzalutamide compared to bicalutamide (Tran et al., 2009), we determined the therapeutic efficacy of enzalutamide on *Pten −/p53*-deficiency-driven CRPC in genetic mouse model. Enzalutamide had minimal or no suppression of *Pten −/p53*-deficiency-driven CRPC in GEMMs, as evidenced by no histopathology changes and no reduction of prostate tumor weight compared to the vehicle-treated controls (Figs. S4A and 4C). These findings from genetic mouse models together with genetic and pharmacologic studies in xenografts (Figs. S3 and S4) collectively support that loss of *Pten* and *p53* in prostate epithelium leads to AR-independent CRPC, which is *de novo* resistant to second generation ADT *in vivo*.

Based on our genetic studies (Wang et al., 2014) and combination therapeutic findings in PC3/UMN-4240P xenograft models, we tested co-targeting HK2-mediated aerobic glycolysis with 2-DG and ULK1-dependent autophagy with CQ for killing ADT-resistant prostate cancer cells to suppress *in situ* prostate tumorigenesis in our autochthonous *Pten −/p53*-deficiency-driven CRPC mouse model by administering PBS (control) or combination of 2-DG and CQ daily for 5 days a week for 4 weeks starting at 12 weeks of age when significant pathological features of invasive prostate cancer were observed (Fig. S5 and (Lu et al., 2015; Xie et al., 2014)). In contrast to lack of efficacy of the ADT, the combination therapy led to a marked reduction in prostate tumor size and weight. Histopathological analysis of combination-treated *Pten*/*p53* double-deficient mice identified significant normal prostate epithelium and a profound normalization of histopathological phenotype that was almost identical to normal prostate (Fig. 6A–C). In line with the mechanistic findings in xenografts, the residual prostate cells

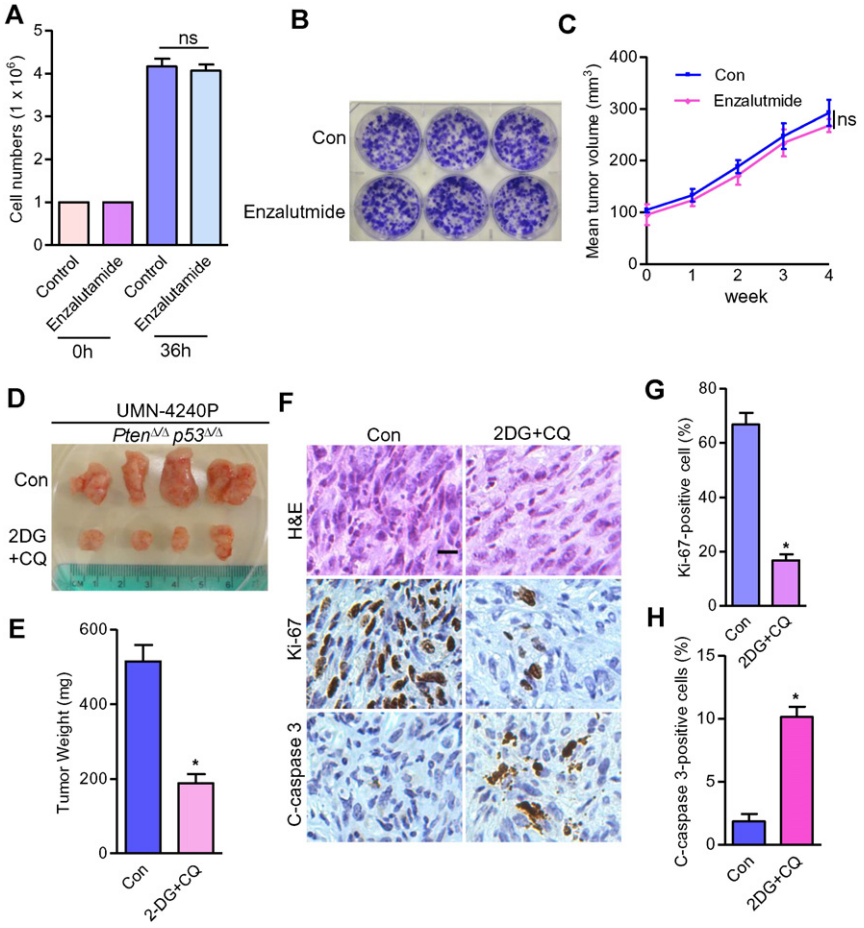

Fig. 5. Co-targeting Warburg effect and autophagy suppresses tumor growth of *Pten* −/*p53*-deficiency-driven CRPC in xenograft models. (A–C) Effects of enzalutamide on prostate cancer cell proliferation and tumor growth in xenograft model: (A) Cell proliferation upon enzalutamide treatment. (B) Colonies were stained by crystal violet after 10 days of cell growth. (C) Tumor growth curve in xenografts carrying UMN-4240P cells treated by vehicle or enzalutamide for 4 weeks. (D–H) Combination therapy with 2-DG and CQ significantly suppresses tumor growth in xenograft mouse models carrying UMN-4240P cells. (D) Representative images of tumor size after 4 weeks of treatment as indicated. (E) Quantification of tumor weight of tumors as shown in (D). (F) Representative hematoxylin/eosin staining, IHC images of Ki-67 and cleaved caspase 3 (C-caspase 3) in tumors from (D) are shown to assess tumor cell proliferation and apoptosis. (G) Quantification of Ki-67 positive cells in tumors shown in (F). (H) Quantification of cleaved caspase 3 positive cells in tumors shown in (F). All data are means ± SEM. *P ≤ 0.01. ns: not statistically significant. Scale bar = 25 μm. See also Fig. S3.

in 2-DG/CQ-treated mice had limited cell proliferation capacity as indicated by the reduction of Ki67-positive cells (Fig. 6D) and increased cleaved-caspase 3-mediated cancer cell apoptosis (Fig. 6E and F). Significantly for selectivity, we did not find appreciable apoptosis in the prostate epithelial cells of 2-DG/CQ-treated age-matched wild-type mice, evident by the lack of cleaved caspase 3 in comparison with 2-DG/CQ-treated *Pten* −/*p53*-deficient mice (Fig. S6A). No notable adverse effect on body weight was observed up to 40 weeks treatment with 2-DG and CQ *in vivo* (Fig. S6B). Notably, the control (vehicle-treated) mice all died in 7 months as previously reported (Chen et al., 2005). However, all the combination-treated mice survived for over one year (Fig. 6G, H), suggesting the long-term *in vivo* treatment with 2-DG plus CQ remarkably extended survival benefit in *Pten* −/*p53*-deficient prostate cancer mouse models.

Therefore, our preclinical studies in *Pten* −/*p53*-deficient prostate cancer mouse models suggest an efficacious and novel therapeutic strategy for the subset of "second generation" ADT-resistant CRPC carrying *PTEN* and *TP53* mutations.

2.8. HK2 as a potential therapeutic target for human CRPC

Our previous studies have shown that HK2 protein abundance is elevated in human prostate cancer tissues, and particularly in human prostate cancers carrying *PTEN* and *TP53* mutations (Wang et al., 2014). Integrative analysis of "Grasso Dataset" (Grasso et al., 2012) using the "cBioPortal" (Cerami et al., 2012; Gao et al., 2013) revealed that mutant *PTEN* co-occurrence with mutant *TP53* was significantly increased compared to wild-type *PTEN* coexisting with mutant *TP53* in CRPC ($P = 0.0235$, X^2 test), and the frequency of co-deletion or -mutation of *PTEN* and *TP53* was 32% (16/50) in CRPC specimens (Fig. 7A). We also examined whether HK2 overexpression could be observed from available CRPC dataset. Since equivalent proteomic data are not yet available for human CRPC specimens, we used mRNA data, despite imperfect correlation between HK2 protein and *HK2* mRNA, by Oncomine analysis of human lethal CRPC dataset (Grasso et al., 2012). *HK2* mRNA was significantly increased in CRPC compared to the primary prostate cancer (PCA) (Fig. 7B). Most importantly, the elevated *HK2* mRNA expression level in CRPC was significantly associated with high mortality of the patients (Fig. 7C) and with reduced survival after first chemotherapy for patients (Fig. 7D). These data suggest that HK2 may serve as a stratification diagnostic and/or prognostic marker and a therapeutic target for CRPC with our combined modality. Therefore, our "proof-of-principle" studies in the preclinical CRPC mouse models provide compelling evidence that co-targeting HK2-mediated Warburg effect with 2-DG and ULK1-dependent autophagy with CQ could be developed into an innovative personalized therapeutic strategy for currently incurable CRPC patients whose tumors have elevated HK2 expression (Fig. 7E).

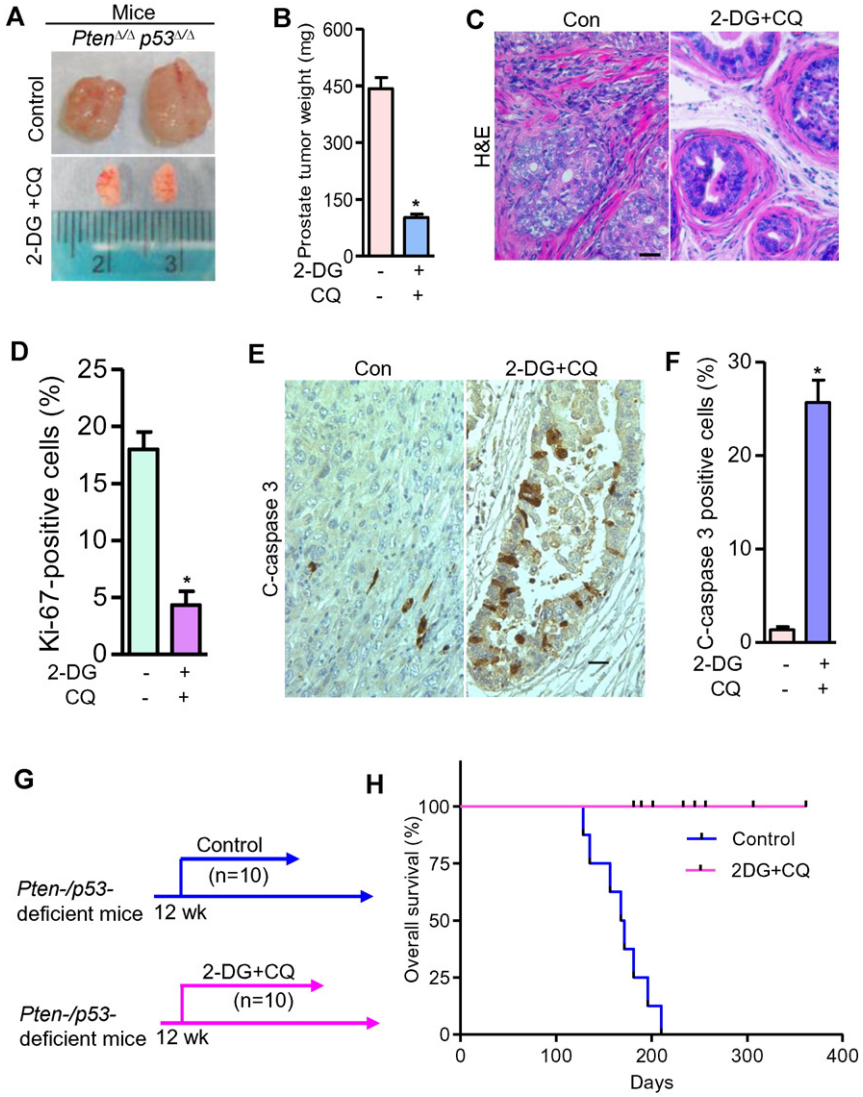

Fig. 6. Co-targeting Warburg effect and autophagy suppresses tumor growth of *Pten* −/*p53*-deficiency-driven CRPC in preclinical mouse models. (A–F) Short-term (4 weeks) combination therapy robustly inhibits prostate tumor growth in *Pten* −/*p53*-deficienent mouse model. (A) Representative images of tumor size of prostate tumor in control and 2-DG plus CQ-treated $Pten^{\Delta/\Delta}p53^{\Delta/\Delta}$ mice at age of 16 weeks. (B) Bar graph showed prostate tumor weight in control and 2-DG plus CQ treated $Pten^{\Delta/\Delta}p53^{\Delta/\Delta}$ mice (n = 6). (C) Representative images of haematoxylin/eosin staining of anterior prostates from D. (D) Quantification of Ki-67 positive cells to assess prostate tumor cell proliferation in control and 2-DG plus CQ treated $Pten^{\Delta/\Delta}p53^{\Delta/\Delta}$ mice. (E) Representative IHC images of cleaved caspase 3 in prostate tumors upon combination treatment. (F) Quantification of cleaved caspase 3 positive cells to assess tumor cell apoptosis from E. (G, H) Long-term *in vivo* combination treatment remarkably extends survival in *Pten* −/*p53*-deficienent mouse model. (G) Treatment schedule. (H) Survival curves of *Pten* −/*p53*-deficienent mouse cohorts treated by vehicle (control) or 2-DG and CQ (n = 10). All data are means ± SEM. *P ≤ 0.01. Scale bar = 25 μm. See also Figs. S4-S6.

3. Discussion

Resistance to the second generation anti-AR axis therapy is a serious therapeutic hurdle for CRPC patients (Claessens et al., 2014). Here we report that loss of *Pten* and *p53* in prostate epithelial cells, occurring in 20–30% of human CRPC, leads to *de novo* murine CRPC that is completely resistant to second generation ADT. In contrast, mechanism-driven co-targeting HK2-mediated Warburg effect with 2-DG and ULK1-dependent autophagy with CQ markedly kill such CRPC cells to suppress tumor growth by selectively inducing apoptosis in multiple independent yet complementary preclinical models.

AMPK is a highly conserved Ser/Thr protein kinase complex that sits at a central node in maintaining cellular energy homeostasis by activating catabolic metabolism and inhibiting anabolic metabolism in response to metabolic stress (Hardie et al., 2012; Oakhill et al., 2012). We have shown here that pharmacological or genetic inhibition of HK2 causes AMPK phosphorylation at Thr 172, an indicator of activated AMPK, which might be due to reduction of ATP ((Patra et al., 2013; Wu et al., 2015). However, the role of activated AMPK in tumorigenesis is less clear, as both oncogenic and tumor suppressor functions have been reported (Liang and Mills, 2013). During cancer treatment, the role of AMPK also remains controversial (Liang and Mills, 2013). The possible reasons might be that catalytically active AMPK phosphorylates a plethora of substrates that transduce multiple signals for various cellular responses associated with tumor development and cancer therapy. Our mechanistic studies revealed that activated AMPK functions as a double-edged sword in prostate cancer cells in response to 2-DG-induced metabolic stress. Activation of AMPK induces ULK1-dependent autophagy to protect cells from apoptosis while concomitantly inhibits mTORC1 signaling to reduce MCL-1 protein synthesis to prime mitochondria for apoptosis. These findings provide a strong theoretical rationale for precision targeting of AMPK downstream ULK1-mediated autophagy, rather than AMPK itself, to achieve desired therapeutic outcome.

Our studies provided compelling evidence to support that pharmacologic co-targeting HK2-mediated Warburg effect with 2-DG and

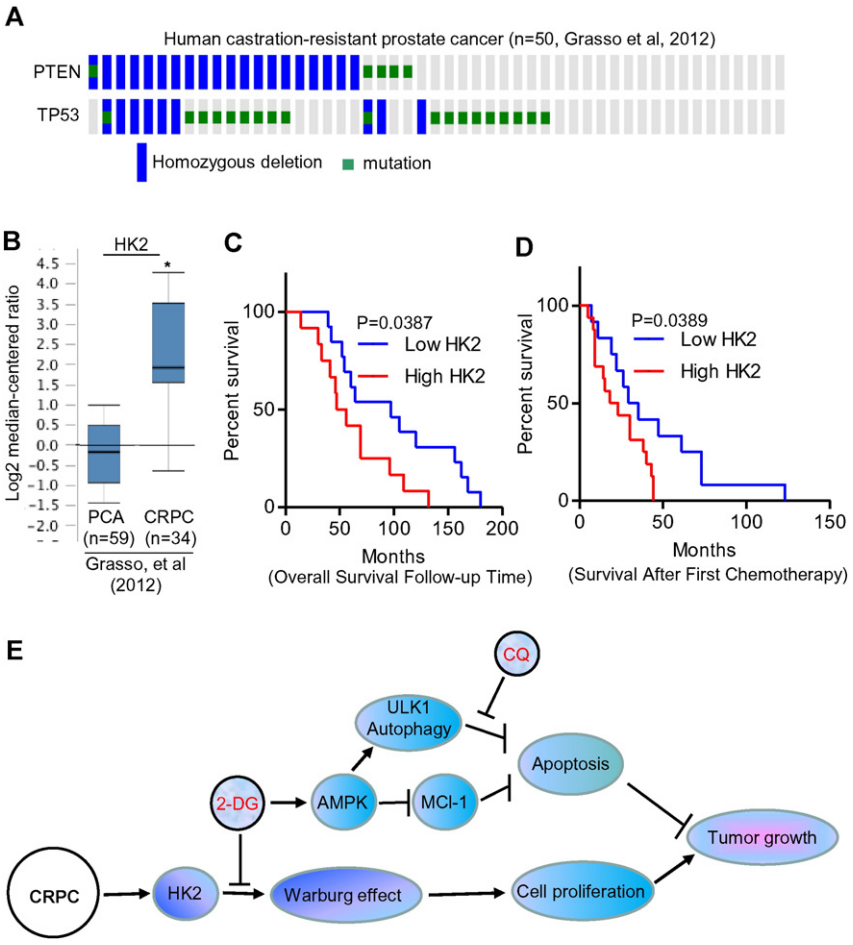

Fig. 7. Expression of HK2 in human CRPC and correlates with patient survival. (A) OncoPrint of mutant frequency of *PTEN* and *TP53* in human castration-resistant prostate cancer. (B) Oncomine boxed plot of HK2 expression at mRNA levels between primary prostate cancer (PCA) and CRPC in dataset Grasso et al. (2012). (C) Correlation between *HK2* mRNA expression level and overall survival follow-up time for CRPC patients. (D) Correlation between *HK2* mRNA expression level and survival after first chemotherapy for CRPC patients. Based on median expression of HK2 in all the CRPC patients from "Grasso dataset", the CRPC patients were separated into high HK2 (above median: Red line) and Low HK2 (Below-median: Blue line) expression. Then, Kaplan–Meier survival analysis of patient cohorts is performed to analyze the survival. The difference of survival is determined by log-rank test. (E) Schematic model depicting co-targeting Warburg effect and autophagy inhibits tumor growth of CRPC *in vivo*. *P ≤ 0.01.

ULK1-induced autophagy with CQ could be an efficacious treatment for *Pten* −/*p53*-deficiency-driven CRPC *in vivo*. Whereas monotherapy with 2-DG or CQ inhibits prostate tumor growth by reducing cell proliferation, combination therapy with 2-DG and CQ causes significant tumor regression by inducing robust cancer cell apoptosis in xenograft models carrying *Pten* −/*p53*-deificient mouse and human prostate cancer cells and in a spontaneous prostate cancer mouse model. Notably, the combination treatment selectively kills cancer cells by apoptosis while sparing normal prostate epithelial cells. This selective cytotoxicity towards *Pten* −/*p53*-deficient CRPC cells is due to their addiction to HK2-mediated Warburg effect for tumor growth (Wang et al., 2014) and their dependence on ULK1-induced autophagy for cell survival when HK2 glycolytic enzyme activity is inhibited.

Interestingly, dataset analyses show that *HK2* is highly expressed in CRPC compared to the primary prostate cancer. Our findings thus provide preclinical proof-of-concept that co-targeting Warburg effect with 2-DG and autophagy with CQ could be extended to effectively treat CRPC patients whose tumors have elevated HK2 expression. Since recent genetic studies revealed that HK2 is required for oncogenic *Kras*-driven lung tumorigenesis and *ErbB2*-driven mammary gland tumorigenesis *in vivo* (Patra et al., 2013), our therapeutic strategy for HK2-mediated prostate cancers may also be extendable to treating HK2-dependent lung and breast cancers.

As far as the tolerability is concerned, accumulating evidence suggests that 2-DG exhibits anti-tumor activity in mouse and rat cancer models *in vivo* at dosages without toxicity to the host animals, including models of sarcomas, adenocarcinomas, leukemias, melanomas, and bladder, colon, lung, and breast tumors (Xi et al., 2014). A recent Phase I clinical trial (NCT00096707) in prostate cancer patients indicated that 2-DG at 63 mg/kg body weight was tolerable dose with anti-tumor effect and was recommended for Phase II clinical Trial (Raez et al., 2013). By allometric scaling, the dosage of 800 mg/kg body weight in mice used for our work here could be converted to a human dose of 65 mg/kg body weight (Reagan-Shaw et al., 2008). Thus, 2-DG dose used in our animal studies approximates the safe range for translation to patients.

The dosage of antimalarial drug CQ and/or its derivatives administrated in our animal studies is also well-tolerated in patients and had been used in patients for decades. Currently, multiple clinical trials targeting autophagy using CQ or its derivate hydroxychloroquine (HCQ) as mono- or combination-therapy for tumors are under way (http://www.cancer.gov/clinicaltrials). Importantly, no notable adverse physiological consequences, monitored by body weight, are observed with long-term administration of 2-DG and CQ in our mouse studies. Thus, building upon insights gained from our findings in the preclinical models and the clinical use knowledge of these two existing drugs, repurposing

them for treating CRPC could be expedited from the bench to bedside. Our studies therefore have immediate implications for the design of clinical trials to evaluate the combination treatment with 2-DG and CQ as a novel targeted therapeutic strategy for the subsets of currently incurable CRPC carrying *PTEN* and *TP53* mutations.

4. Materials and methods

4.1. Generation and genotyping of Pten and/or p53 mutant mice

Experimental procedures were performed as previously described (Wang et al., 2014). Conditional $Pten^{flox/flox}$ mouse was generated as previously described (Zheng et al., 2008). The conditional $p53^{flox/flox}$ mouse was generously provided by Dr. A Berns (Jonkers et al., 2001). *PB-Cre4* transgenic mice were obtained from the NCI Mouse Repository. Female mice carrying $Pten^{flox/+}p53^{flox/+}$ were crossed with male mice harboring $PB\text{-}Cre4^{+}\,Pten^{flox/+}p53^{flox/+}$ to generate mutant mice with prostate epithelium-specific deletion of *Pten* and/or *p53*. DNA from tail or prostate tumors was used for PCR-based genotyping as reported (Wang et al., 2014). All animal protocols were reviewed and approved by the University of Minnesota Institutional Animal Care and Use Committee.

4.2. Genotyping PCR reactions

For *PB-Cre4*: Primer 1 (5′-TCT GCA CCT TGT CAG TGA GG-3′) and primer 2 (5′-GCA AAC GGA CAG AAG CAT TT-3′) were used. Thermocycling conditions were 28 cycles of 94 °C for 45 s, 55 °C for 30 s and 72 °C for 1 min.

For $p53^{Flox/Flox}$: Primer1 (5′-CAC AAA AAC AGG TTA AAC CCA G-3′) and primer 2 (5′-AGC ACA TAG GAG GCA GAG AC-3′) were used. To detect the deleted allele, D*p53* primer (5′-GAA GAC AGA AAA GGG GAG GG-3′) and primer 1 were used. Thermo cycling conditions were 35 cycles of 94 °C for 1 min, 60 °C for 45 s and 72 °C for 30 s.

For $Pten^{Flox/Flox}$: Primer 1 (5′-CTT CGG AGC ATG TCT GGC AAT GC-3′) and primer 2 (5′-CTG CAC GAG ACT AGT GAG ACG TGC-3′) were used. To detect the deleted allele, D*Pten* primer (5′-AAG GAAGAG GGT GGG GAT AC-3′) and primer 1 were used. Thermo cycling conditions were 30 cycles of 94 °C for 1 min, 62 °C for 45 s and 72 °C for 1 min.

4.3. Chemical compounds

Chemicals were obtained from the following sources: 2-Deoxyglucose (2-DG) and chloroquine (CQ), Sigma-Aldrich. Enzalutamide, Selleck or APExBio. 2-DG and CQ were dissolved in PBS, at 1000 times the final concentration used *in vitro*, and the freshly prepared 2-DG and CQ were administered to mice by intraperitoneal injection at 800 mg/kg and 50 mg/kg *in vivo*, respectively. Enzalutamide was dissolved in DMSO at 1000 times the final concentration used in experiments *in vitro*, and Enzalutamide was dissolved in vehicle (1% carboxymethyl cellulose, 0.1% Tween-80, 5% DMSO) and given at a dose of 30 mg/kg by oral gavage in mice.

4.4. Cell culture

RWPE-1 immortalized non-tumorigenic human prostate cells and human prostate cancer cell lines (PC3, LNCaP and DU145) were obtained from American Type Culture Collection. RWPE-1 cells were maintained in Keratinocyte Serum Free Medium (K-SFM). PC3 cells were maintained in F-12K supplemented with 10% fetal bovine serum. LNCaP and DU145 cells were maintained in RPMI-1640 supplemented with 10% fetal bovine serum. Mouse tumor derived polyclonal cancer cells (UMN-4240P) were grown in DMEM containing 10% FBS at standard tissue culture condition.

4.5. Cell viability and clonogenic survival assay

For cell viability assay, each well of a 12-well plate was seeded with 2×10^5 cells and the plates were incubated overnight to allow cells to attach. After 48 h of drug treatment, the cell viability was determined by trypan blue. For clonogenic survival assay, cells were plated in triplicate at 2×10^4 cells per well of six-well tissue culture plate. After one to two weeks of growth, cell colonies were fixed in 10% formalin and stained with crystal violet (0.05% *w*/*v*).

4.6. Cell cycle analysis

Cells were harvested, fixed in ethanol, incubated with ribonuclease and stained with propidium iodide. DNA content was determined on a FACScan flow cytometer (Beckman Coulter).

4.7. Glucose consumption and lactate production

PC3 cells were seeded at 1×10^5 cells per well in a 6-well plate and incubated for 24 h to allow the cells to attach. The cells were then treated with vehicle only or 2-DG (20 mM) for 48 h. The glucose and lactate concentrations in the medium during a period of 72 h were determined using the Glucose Assay Kit (Eton Bioscience) and Lactate Assay Kit II (Biovision), respectively. Glucose consumption was determined by the difference between the original glucose concentration and the measured glucose concentration at 72 h. As the medium itself does not contain lactate, the measured lactate concentration reflects the lactate production by the cells. The values of glucose consumption and lactate production were converted into actual rate.

4.8. Drug treatment in animal models

Xenograft mouse models carrying human prostate cancer PC3 cells or mouse prostate cancer UMN-4240P cells were established in male NSG mice as described (Wang et al., 2014). Treatment started once xenograft tumors were established (the tumor volume reaches 50–100 mm^3). For PC3 xenografts, mice were randomly assigned into four groups and treated with PBS (Control), 2-DG (800 mg/kg in PBS), CQ (50 mg/kg in PBS), or 2-DG (800 mg/kg) plus CQ (50 mg/kg) by intraperitoneal injection (I.P.), daily for 5 days a week for 4 weeks. For mice carrying xenografts of UMN-4240P cells, two groups were randomly assigned and treated with PBS (Control) or 2-DG (800 mg/kg) plus CQ (50 mg/kg) as described in xenograft models harboring PC3 cells. Then, the NSG mice carrying xenografts were euthanized and the tumors were dissected, weighed and processed for histopathology and biochemical analyses. To observe the short-term therapeutic efficacy in genetically engineered castration resistant prostate cancer mouse model, six *Pten*/*p53*-deficient mice at age of 12-weeks per group were treated with PBS (Control) or 2-DG (800 mg/kg) plus CQ (50 mg/kg) by I.P., daily for 5 days a week for 4 weeks. Mice were euthanized, and prostate tumors were dissected, weighed and processed for histopathology and biochemical analyses at the conclusion of these studies. To determine survival benefit upon long-term treatment, ten *Pten*/*p53*-deficient mice at age of 12-weeks per group were treated with PBS (Control) or 2-DG (800 mg/kg) plus CQ (50 mg/kg) by I.P., daily for 5 days a week until the mice were found moribund.

4.9. Androgen deprivation therapy in mice

For ADT in xenograft mouse models: male NSG mice at 10 weeks of age were castrated by surgically removing the testes. After 2 weeks, the UMN-4240P cells were injected into the flank of non-castrated and surgical castrated male NSG mice; or the UMN-4240P cells stably expressing lentivirus-mediated shRNAs for *Ar* or empty vector (control) were implanted into the flanks of male castrated NSG mice; or the NSG mice carrying xenografts with tumor size reached approximately

100 mm^3 were randomly assigned into two groups and treated with vehicle (control) or enzalutamide at a dose of 30 mg/kg by oral gavage as reported (Tran et al., 2009), daily for 5 days a week for 4 weeks and tumor growth was monitored. Tumor size was measured weekly in 2 dimensions (l × w) with calipers and calculated by the following formula: volume = (length × $width^2$)/2. At the endpoint of each experiment, the NSG mice carrying xenografts were euthanized and the tumors were dissected, weighed and processed for histopathology and biochemical analyses. For ADT in genetic mouse model, *Pten*/*p53*-deficient mice at 12 weeks of age were castrated by surgically removing the testes or by using enzalutamide at a dose of 30 mg/kg by oral gavage as reported (Tran et al., 2009), daily for 5 days a week for 4 weeks. Mice were euthanized, and prostate tumors were dissected, weighed and processed for histopathology and biochemical analyses at the conclusion of these studies.

4.10. Immunoblotting

Cells were lysed with TEB150 buffer (50 mM HEPES pH 7.4, 150 mM NaCl, 2 mM $MgCl_2$, 5 mM EGTA pH 8.0, 1 mM dithiothreitol, 0.5% Triton X–100, 10% glycerol, 1 mM Na_3VO_4, 1 μM microcystin–LR and protease/phosphatase inhibitor cocktail). Lysates from mouse prostates were prepared by homogenizing mouse prostates in modified RIPA buffer (20 mM Tris–HCl pH 7.4, 150 mM NaCl, 1% NP-40, 5 mM EDTA and protease/phosphatase inhibitor cocktail). Insoluble material was removed by centrifugation. Proteins were resolved by SDS-PAGE and transferred to polyvinylidene difluoride membranes. Membranes were blocked with 5% non-fat milk in phosphate-buffered saline and then probed with the appropriate primary antibody in 5% non-fat milk overnight at 4 °C [AMPKα, phospho-AMPKα (Thr172), Bax, cleaved PARP, cleaved caspase-3, Hexokinase 2, ATG5, ATG7, Beclin 1, ULK1, and LC3-II from Cell Signaling; β Tubulin (G-8) and Bcl-2 (N-19) from Santa Cruz Biotechnology; AR for IHC from Millipore and AR for Western blot from Santa Cruz; and LC3 (M115–3) from MBL International Corporation]. Subsequently, membranes were washed in phosphate-buffered saline with 0.3% Tween 20, and incubated with secondary antibody conjugated to horseradish peroxidase. Proteins were visualized by enhanced chemiluminescence.

4.11. Immunohistochemistry (IHC)

All immunohistochemical analyses were conducted as previously described (Wang et al., 2009). The following antibodies were used: HK2, cleaved caspase-3, p-AMPK(Thr172), and LC3B (LC3II) from Cell Signaling; Ki-67 from Thermo Scientific; AR from Millipore.

4.12. Plasmids and viral transfections

pQCXIP-GFP-LC3 was constructed by inserting GFP-LC3 into *BamH*1 and *EcoR*I restriction sites of pQCXIP vector and verified by DNA sequencing. pcDNA-Bcl2 were generated using methods previously described (Deng et al., 2003). All shRNAs were obtained from the BioMedical Genomics Center at The University of Minnesota. These are lentiviral shRNAs and are as follows: human PTEN (TRCN0000002747 and TRCN0000002749), human ULK1 (TRCN0000000835 and TRCN 0000000836), human AMPK (TRCN0000000857 and TRCN00 00000858), human Bax (TRCN0000033470 and TRCN0000033471), HK2 (TRCN0000037670 and TRCN0000037673 for human; TRCN0 000012545 and TRCN0000012546 for mouse), human ATG5 (TRCN0000151963 and TRCN0000150645), human ATG7 (TRCN00 00007584 and TRCN0000007585), human Beclin1 (TRCN0000033549 and TRCN0000033552), and human p70SRK (TRCN0000022904 and TRCN0000022907). The negative control vector was the pLKO.1 vector backbones that has no hairpin insert. shRNA-encoding plasmids were co-transfected with envelope and packaging plasmids (VSVG, REV and pMDL) into actively growing HEK-293 T cells using the calcium phosphate transfection method. Virus-containing supernatants were collected 36 h after transfection, centrifuged to remove cell debris and filtered to eliminate cells. The target cells were infected in the presence of 8 μg/ml polybrene. Cells were selected with 8 μg/ml puromycin 24 h later to generate stable cell lines and knockdown efficiency was confirmed by immunoblotting.

4.13. Statistical analyses

Statistical comparisons were analyzed by ANOVA (greater than two groups) or Student's *t* test (two groups only) with Graphad Prism (v.5). The difference in survival is determined by log-rank test. Data are expressed as means ± SEM. Statistical significances were accepted at $p < 0.05$.

Author contributions

L. W. performed therapeutic studies for animals, hematoxylin and eosin staining, and immunohistochemistry on tumor samples. J.W. performed cell culture and tumor xenograft studies. H.X., F.W., C.J., Y.Z. X.G., H.W and SM helped with the cell culture and animal experiments, and generated data or provided reagents. F.W. also performed bioinformatics analyses. J.L. provided conceptual advices, assisted with the design of animal experiments and data intepretation, and edited the manuscript. Y.D. conceived the project, designed the experiments, analyzed and interpreted the data, wrote and edited the manuscript.

Disclosure of potential conflicts of interest

No potential conflicts of interest were disclosed.

Acknowledgements

This work was supported, in part, by grants from the US National Cancer Institute (R01 CA160333, Y.D; R21 CA155522, Y.D. and J.L; R01 CA172169, J.L. and Y.D), The University of Minnesota Grant-in Aid (Y.D.) and start-up funds from The Hormel Foundation (Y.D.).

Appendix A. Supplementary data

Supplementary data to this article can be found online at http://dx.doi.org/10.1016/j.ebiom.2016.03.022.

References

Cerami, E., Gao, J., Dogrusoz, U., Gross, B.E., Sumer, S.O., Aksoy, B.A., Jacobsen, A., Byrne, C.J., Heuer, M.L., Larsson, E., et al., 2012. The cBio cancer genomics portal: an open platform for exploring multidimensional cancer genomics data. Cancer Discov. 2, 401–404.

Chen, C.D., Welsbie, D.S., Tran, C., Baek, S.H., Chen, R., Vessella, R., Rosenfeld, M.G., Sawyers, C.L., 2004. Molecular determinants of resistance to antiandrogen therapy. Nat. Med. 10, 33–39.

Chen, Z., Trotman, L.C., Shaffer, D., Lin, H.K., Dotan, Z.A., Niki, M., Koutcher, J.A., Scher, H.I., Ludwig, T., Gerald, W., et al., 2005. Crucial role of p53-dependent cellular senescence in suppression of Pten-deficient tumorigenesis. Nature 436, 725–730.

Claessens, F., Helsen, C., Prekovic, S., Van den Broeck, T., Spans, L., Van Poppel, H., Joniau, S., 2014. Emerging mechanisms of enzalutamide resistance in prostate cancer. Nat. Rev. Urol.

de Bono, J.S., Oudard, S., Ozguroglu, M., Hansen, S., Machiels, J.P., Kocak, I., Gravis, G., Bodrogi, I., Mackenzie, M.J., Shen, L., et al., 2010. Prednisone plus cabazitaxel or mitoxantrone for metastatic castration-resistant prostate cancer progressing after docetaxel treatment: a randomised open-label trial. Lancet 376, 1147–1154.

de Bono, J.S., Logothetis, C.J., Molina, A., Fizazi, K., North, S., Chu, L., Chi, K.N., Jones, R.J., Goodman Jr., O.B., Saad, F., et al., 2011. Abiraterone and increased survival in metastatic prostate cancer. N. Engl. J. Med. 364, 1995–2005.

DeMarzo, A.M., Nelson, W.G., Isaacs, W.B., Epstein, J.I., 2003. Pathological and molecular aspects of prostate cancer. Lancet 361, 955–964.

Deng, Y., Ren, X., Yang, L., Lin, Y., Wu, X., 2003. A JNK-dependent pathway is required for TNFalpha-induced apoptosis. Cell 115, 61–70.

Gao, J., Aksoy, B.A., Dogrusoz, U., Dresdner, G., Gross, B., Sumer, S.O., Sun, Y., Jacobsen, A., Sinha, R., Larsson, E., et al., 2013. Integrative analysis of complex cancer genomics and clinical profiles using the cBioPortal. Sci. Signal. 6, pl1.

Gao, D., Vela, I., Sboner, A., Iaquinta, P.J., Karthaus, W.R., Gopalan, A., Dowling, C., Wanjala, J.N., Undvall, E.A., Arora, V.K., et al., 2014. Organoid cultures derived from patients with advanced prostate cancer. Cell 159, 176–187.

Grasso, C.S., Wu, Y.M., Robinson, D.R., Cao, X., Dhanasekaran, S.M., Khan, A.P., Quist, M.J., Jing, X., Lonigro, R.J., Brenner, J.C., et al., 2012. The mutational landscape of lethal castration-resistant prostate cancer. Nature 487, 239–243.

Haffner, M.C., Mosbruger, T., Esopi, D.M., Fedor, H., Heaphy, C.M., Walker, D.A., Adejola, N., Gurel, M., Hicks, J., Meeker, A.K., et al., 2013. Tracking the clonal origin of lethal prostate cancer. J. Clin. Invest. 123, 4918–4922.

Hardie, D.G., Ross, F.A., Hawley, S.A., 2012. AMPK: a nutrient and energy sensor that maintains energy homeostasis. Nat. Rev. Mol. Cell Biol. 13, 251–262.

Jonkers, J., Meuwissen, R., van der Gulden, H., Peterse, H., van der Valk, M., Berns, A., 2001. Synergistic tumor suppressor activity of BRCA2 and p53 in a conditional mouse model for breast cancer. Nat. Genet. 29, 418–425.

Kim, J., Kundu, M., Viollet, B., Guan, K.L., 2011. AMPK and mTOR regulate autophagy through direct phosphorylation of Ulk1. Nat. Cell Biol. 13, 132–141.

Liang, J., Mills, G.B., 2013. AMPK: a contextual oncogene or tumor suppressor? Cancer Res. 73, 2929–2935.

Lu, W., Liu, S., Li, B., Xie, Y., Adhiambo, C., Yang, Q., Ballard, B.R., Nakayama, K.I., Matusik, R.J., Chen, Z., 2015. SKP2 inactivation suppresses prostate tumorigenesis by mediating JARID1B ubiquitination. Oncotarget 6, 771–788.

Lunardi, A., Ala, U., Epping, M.T., Salmena, L., Clohessy, J.G., Webster, K.A., Wang, G., Mazzucchelli, R., Bianconi, M., Stack, E.C., et al., 2013. A co-clinical approach identifies mechanisms and potential therapies for androgen deprivation resistance in prostate cancer. Nat. Genet. 45, 747–755.

Markert, E.K., Mizuno, H., Vazquez, A., Levine, A.J., 2011. Molecular classification of prostate cancer using curated expression signatures. Proc. Natl. Acad. Sci. U. S. A. 108, 21276–21281.

Mathew, R., Karantza-Wadsworth, V., White, E., 2007. Role of autophagy in cancer. Nat. Rev. Cancer 7, 961–967.

Mills, J.R., Hippo, Y., Robert, F., Chen, S.M., Malina, A., Lin, C.J., Trojahn, U., Wendel, H.G., Charest, A., Bronson, R.T., et al., 2008. mTORC1 promotes survival through translational control of mcl-1. Proc. Natl. Acad. Sci. U. S. A. 105, 10853–10858.

Mizushima, N., Yoshimori, T., Levine, B., 2010. Methods in mammalian autophagy research. Cell 140, 313–326.

Oakhill, J.S., Scott, J.W., Kemp, B.E., 2012. AMPK functions as an adenylate charge-regulated protein kinase. Trends Endocrinol. Metab. 23, 125–132.

Ohsumi, Y., 2001. Molecular dissection of autophagy: two ubiquitin-like systems. Nat. Rev. Mol. Cell Biol. 2, 211–216.

Patra, K.C., Wang, Q., Bhaskar, P.T., Miller, L., Wang, Z., Wheaton, W., Chandel, N., Laakso, M., Muller, W.J., Allen, E.L., et al., 2013. Hexokinase 2 is required for tumor initiation and maintenance and its systemic deletion is therapeutic in mouse models of cancer. Cancer Cell.

Petrylak, D.P., Tangen, C.M., Hussain, M.H., Lara Jr., P.N., Jones, J.A., Taplin, M.E., Burch, P.A., Berry, D., Moinpour, C., Kohli, M., et al., 2004. Docetaxel and estramustine compared with mitoxantrone and prednisone for advanced refractory prostate cancer. N. Engl. J. Med. 351, 1513–1520.

Raez, L.E., Papadopoulos, K., Ricart, A.D., Chiorean, E.G., Dipaola, R.S., Stein, M.N., Rocha Lima, C.M., Schlesselman, J.J., Tolba, K., Langmuir, V.K., et al., 2013. A phase I dose-escalation trial of 2-deoxy-D-glucose alone or combined with docetaxel in patients with advanced solid tumors. Cancer Chemother. Pharmacol. 71, 523–530.

Reagan-Shaw, S., Nihal, M., Ahmad, N., 2008. Dose translation from animal to human studies revisited. FASEB J. 22, 659–661.

Robinson, D., Van Allen, E.M., Wu, Y.M., Schultz, N., Lonigro, R.J., Mosquera, J.M., Montgomery, B., Taplin, M.E., Pritchard, C.C., Attard, G., et al., 2015. Integrative clinical genomics of advanced prostate cancer. Cell 161, 1215–1228.

Rubinsztein, D.C., Gestwicki, J.E., Murphy, L.O., Klionsky, D.J., 2007. Potential therapeutic applications of autophagy. Nat. Rev. Drug Discov. 6, 304–312.

Ryan, C.J., Smith, M.R., de Bono, J.S., Molina, A., Logothetis, C.J., de Souza, P., Fizazi, K., Mainwaring, P., Piulats, J.M., Ng, S., et al., 2013. Abiraterone in metastatic prostate cancer without previous chemotherapy. N. Engl. J. Med. 368, 138–148.

Scher, H.I., Beer, T.M., Higano, C.S., Anand, A., Taplin, M.E., Efstathiou, E., Rathkopf, D., Shelkey, J., Yu, E.Y., Alumkal, J., et al., 2010. Antitumour activity of MDV3100 in castration-resistant prostate cancer: a phase 1–2 study. Lancet 375, 1437–1446.

Scher, H.I., Fizazi, K., Saad, F., Taplin, M.E., Sternberg, C.N., Miller, K., de Wit, R., Mulders, P., Chi, K.N., Shore, N.D., et al., 2012. Increased survival with enzalutamide in prostate cancer after chemotherapy. N. Engl. J. Med. 367, 1187–1197.

Thoreen, C.C., Chantranupong, L., Keys, H.R., Wang, T., Gray, N.S., Sabatini, D.M., 2012. A unifying model for mTORC1-mediated regulation of mRNA translation. Nature 485, 109–113.

Tran, C., Ouk, S., Clegg, N.J., Chen, Y., Watson, P.A., Arora, V., Wongvipat, J., Smith-Jones, P.M., Yoo, D., Kwon, A., et al., 2009. Development of a second-generation antiandrogen for treatment of advanced prostate cancer. Science 324, 787–790.

Wang, L., Bonorden, M.J., Li, G.X., Lee, H.J., Hu, H., Zhang, Y., Liao, J.D., Cleary, M.P., Lu, J., 2009. Methyl-selenium compounds inhibit prostate carcinogenesis in the transgenic adenocarcinoma of mouse prostate model with survival benefit. Cancer Prev. Res. 2, 484–495.

Wang, L., Xiong, H., Wu, F., Zhang, Y., Wang, J., Zhao, L., Guo, X., Chang, L.J., Zhang, Y., You, M.J., et al., 2014. Hexokinase 2-mediated warburg effect is required for PTEN- and p53-deficiency-driven prostate cancer growth. Cell Rep. 1461–1474.

Wu, Y., Sarkissyan, M., McGhee, E., Lee, S., Vadgama, J.V., 2015. Combined inhibition of glycolysis and AMPK induces synergistic breast cancer cell killing. Breast Cancer Res. Treat. 151, 529–539.

Xi, H., Kurtoglu, M., Lampidis, T.J., 2014. The wonders of 2-deoxy-D-glucose. IUBMB Life 66, 110–121.

Xie, Y., Liu, S., Lu, W., Yang, Q., Williams, K.D., Binhazim, A.A., Carver, B.S., Matusik, R.J., Chen, Z., 2014. Slug regulates E-cadherin repression via p19Arf in prostate tumorigenesis. Mol. Oncol. 8, 1355–1364.

Zheng, H., Ying, H., Yan, H., Kimmelman, A.C., Hiller, D.J., Chen, A.J., Perry, S.R., Tonon, G., Chu, G.C., Ding, Z., et al., 2008. p53 and Pten control neural and glioma stem/progenitor cell renewal and differentiation. Nature 455, 1129–1133.